Lipids modulate the conformational dynamics of a secondary multidrug transporter

Article:
Martens, C, Stein, RA, Masureel, M et al. (7 more authors) (2016) Lipids modulate the conformational dynamics of a secondary multidrug transporter. Nature Structural & Molecular Biology, 23 (8). pp. 744-751. ISSN 1545-9993

https://doi.org/10.1038/nsmb.3262

Lipid headgroups modulate the conformational dynamics of the secondary multidrug transporter LmrP.

Chloé Martens[1], Richard A Stein[2], Matthieu Masureel[1], Smriti Mishra[2], Albert Konijnenberg[4], Frank Sobott[4], Cédric Govaerts[1,5] and Hassane S Mchaourab[2,5].

[1]Laboratory for the Structure and Function of Biological Membranes, Center for Structural Biology and Bioinformatics, Université Libre de Bruxelles, CP 206/02, Bd du Triomphe, 1050 Brussels, Belgium

[2]Department of Molecular Physiology and Biophysics, Vanderbilt University Medical Center, 2215 Garland Avenue, Nashville, TN 37232, USA

[4]Department of Chemistry, Biomolecular & Analytical Mass Spectrometry group, University of Antwerp, Antwerp, Belgium

[5]These authors are co-last authors

Correspondence should be addressed to C.G. (cedric.govaerts@ulb.ac.be) and H.M. (hassane.mchaourab@vanderbilt.edu)

Abstract

Direct interactions with lipids have emerged as key determinants of the folding, structure and function of membrane proteins, but an understanding of how lipids modulate protein dynamics is still lacking. Here, we systematically explored the effects of lipids on the conformational dynamics of the proton-powered, multidrug transporter LmrP utilizing the pattern of distances between spin label pairs previously shown to fingerprint alternating access of the protein. We uncover at the molecular level how the lipid headgroups shape the conformational energy landscape of the transporter. The model emerging from our data hypothesizes a direct interaction between lipid headgroups and a conserved motif of charged residues that control the conformational equilibrium through an interplay of electrostatic interactions within the protein. Together, our data lay the foundation for a comprehensive model of secondary multidrug transport in lipid bilayers.

There is overwhelming consensus that the biological membrane must play a critical role in membrane protein structure, stability and function owing to its unique physicochemical properties such as dielectric constant, lateral pressure, curvature and thickness [1-6]. It has long been recognized, primarily from crystal structures, that lipid molecules directly interact with membrane proteins with high affinity [7-9]. However, only recently did direct experimental evidence reveal that bound lipids can affect folding, impart stability and modulate the function and physiological role of membrane proteins [10-15]. For example, lipids act as allosteric modulators of the β2 adrenergic receptor activation by its cognate ligands [16]. In dopamine-mediated neurotransmission, the lipid PIP_2 controls signaling events associated with physiological and behavioral consequences [17] and computational models have hypothesized interactions of PIP_2 with specific structural elements of neurotransmitter transporters [18,19]. Because most membrane proteins undergo transitions between distinct conformations, the lipid modulation of their function must be underpinned by direct effects on the underlying

dynamics [20]. However, to our knowledge, a detailed analysis of how lipids shape the conformational energy landscape of a membrane protein has not been carried out.

Here we elucidate the mechanism by which specific lipid molecules modulate the stability of distinct states of the multidrug transporter LmrP from *Lactococcus lactis*. LmrP, a member of the Major Facilitator Superfamily (MFS), couples the downhill translocation of protons along their transmembrane gradient to the uphill transport of hydrophobic cytotoxic compounds [21-23]. Unlike substrate-specific MFS transporters, multidrug antiporters have evolved to be polyspecific and to potentially bind their substrates from the inner leaflet of the bilayer [24,25]. Their ability to bind structurally and chemically dissimilar substrates challenge the notions of high-affinity substrate binding and strict ion-substrate coupling [26-28]. Furthermore, the active efflux of diverse cytotoxic compounds through secondary multidrug transporters contributes to bacterial antibiotic resistance [25,29,30]. In this context, an accurate description of the mechanism of these transporters in a native-like environment would be valuable from a fundamental as well as a clinical standpoint.

We recently described the proton- and substrate-dependent alternating access of LmrP in detergent micelles [31] using a systematic DEER analysis of distances between spin label pairs on the extracellular and intracellular sides of the transporter [32]. We identified two conformations of LmrP in equilibrium: outward-facing poised to bind protons and inward-facing from which protons are released. Mapping of the structural rearrangements at basic and acidic pH values established that the protonation state of key acidic residue(s) is the main trigger for the transition between outward-open and inward-open conformations. Specifically a conserved aspartate (D68) was shown to control the energetics of the equilibrium between the two conformations. Residue 68 is part of the signature motif of the MFS [33] and is highly conserved across different organisms [25]. In parallel, a structure of the MFS drug transporter, YajR, identified this residue as a key contributor to the stability of the outward-facing conformation trapped in the crystal [34].

In this work, we demonstrate in unprecedented details how specific interactions between lipid headgroups and a conserved network of charges shift the proton- and substrate-dependent equilibrium between inward- and outward-facing conformations of LmrP. DEER distance measurements were carried out using selected spin label pairs of the transporter reconstituted in nanodiscs [35] of varying lipid compositions. We found that while the two conformations identified in detergent micelles persists in lipid bilayers, the apparent pK of the conformational transition is shifted by close to two pH units. This shift appears to be the consequence of lipid headgroup-dependent stabilization of the inward-facing conformation. To dissect the origin of selective preference for this conformation in lipids, we carried out a systematic mutagenesis of residues in a charge network hypothesized to modulate the interactions which stabilize the outward-facing conformation. Our data suggest a model in which lipid headgroups interact with this charge network thereby stabilizing an inward-facing conformation.

Results

Conformational dynamics of LmrP in lipid bilayers

We monitored the ligand-dependent conformational changes of LmrP in lipid bilayers by distance measurements of spin labeled cysteine mutants reconstituted in nanodiscs. Twelve double cysteines mutants, six on each of the cytoplasmic and extracellular sides of the transmembrane helices (TMs), were selected based on previous results and predictions from homology models [31]. On each side, four cysteine pairs probe distances between the N- and C-terminal lobes, while the other two pairs are located within the same lobe. Following verification of the stability and functional integrity of the mutants (Supplementary Fig.6 and [31]), they were reconstituted in nanodiscs composed of *E.coli* polar lipids (see Methods) which were previously shown to support proton-coupled transport by LmrP [36,37].

Since LmrP utilizes proton translocation down a transmembrane gradient to power the transport of structurally dissimilar substrates, we studied the structural rearrangements induced by changes in proton concentration (i.e. changes in pH) or following addition of LmrP substrates, either Hoechst 33342 or Ethidium Bromide (EtBr). For this purpose, distance measurements were carried out at pH8 (low proton concentration), pH6 (high proton concentration) and pH8 with substrate. We observed that an increase in proton concentration or addition of Hoechst 33342 results in major structural rearrangements between the N- and C-terminal lobes (Fig.1). Low pH suppresses the long distance component on the extracellular side (Fig.1 a), concomitant with a shift in the distributions on the cytoplasmic side (Fig.1 b) to a pattern characteristic of the inward-facing conformation reported previously [31]. The pattern of distance changes observed in the presence of the substrate Hoechst 33342 is opposite to that at low pH demonstrating that substrate binding favors the outward-open conformation (Fig.1 a-b).

By comparison, the pairs within the same lobe show minor changes at low pH or upon addition of Hoechst 33342 (Supplementary Fig.1), with the exception of the TM4-TM5 extracellular pair (Supplementary Fig.1 a) and the TM8-TM11 cytoplasmic pair

(Supplementary Fig.1 b). We note that the LmrP substrate EtBr barely alters the distance distributions (Supplementary Fig.2 and Supplementary Fig.1 c), demonstrating a specificity of the conformational changes to the binding of Hoechst 33342. To demonstrate that EtBr binds LmrP, distance measurements were carried out using the TM10-TM8 pair, previously shown to be sensitive to the presence of bound substrate(s) [31]. In the absence of EtBr, the distance distribution is broad and the peaks are poorly defined. However, in the presence of EtBr, the distance distribution displays a narrow peak, indicative of a local ordering of LmrP upon substrate binding (Supplementary Fig.2).

Reconstitution of LmrP in lipid bilayers stabilizes the inward-open conformation

While the sign and amplitude of the substrate and pH-dependent distance changes are consistent with those previously reported in detergent micelles [31], the presence of the lipid bilayer shifts the conformational equilibrium towards the inward-facing conformation at both pH values in Fig.1. To investigate the origin of this change in equilibrium, we systematically compared the pH-dependence of the distance distributions in nanodiscs to that obtained in detergent micelles. Distance measurements were performed in the pH range from 4.5 to 8.5 using one distance reporter on each of the extracellular and cytoplasmic sides of the transporter (Fig.2). Visual inspection of the distance distributions for both reporters shows that, at all pH values, the component(s) characteristic of the inward-open conformation are largely dominant when the transporter is reconstituted into lipids, compared to the transporter in detergent micelles.

To obtain a pH titration curve, the changes in amplitude of the distance components, each representing a conformational state, were quantitatively determined by global analysis of the raw DEER decays for the same spin label pair at different pH values (see Methods). This fitting procedure assumes that the same components (defined by the average distance and the width) are present in each dataset, but their amplitudes are allowed to vary in response to different biochemical conditions (i.e. pH) [38,39]. The resulting titration curve, depicting the population of the inward-open component (Fig.3) versus pH, has a typical

sigmoidal shape with an inflection point at the apparent pK of the transition from one state to the other. On the extracellular side, the apparent pK is 4.7±0.3 for the detergent solubilized protein and increases to 6.9 ±0.2 in bilayers of *E.coli* polar lipids (Fig.3 left panels). On the cytoplasmic face, this value is 5.9±0.2 in detergent micelles and 7.3 ±0.1 in the lipid bilayers (Fig.3 right panels). Thus, lipids are a determinant of the pH-sensitivity of the global conformational transition of LmrP.

A charge network controls the conformational preferences in lipid bilayers

We have previously shown that, in detergent micelles, the pH dependence of the conformational equilibrium is determined to a large extent by the protonation state of the highly conserved residue D68 [31]. A structural interpretation of this result emerged from analysis of the crystal structure of YajR [34], a homolog of LmrP captured in an outward-open conformation. It was observed that this conformation is stabilized by an interaction between the conserved aspartate (residue 73 in YajR) at the cytoplasmic end of helix 2 and the backbone of helix 11 (Fig.4 a) in the context of a conserved charge-relay network consisting of D73-R77-D126 (D68-R72-D128 in LmrP).

To test if electrostatic interactions in this network of residues contribute to the pH dependence of LmrP conformational change, residues D68 and D128 were mutated to asparagine, in order to mimic permanent protonation. Residue R72 was mutated to a lysine in order to disrupt the interaction between the guanidinium moiety and D68 and D128 postulated from the YajR structure (Fig.4 a). DEER distance measurements were carried out on the detergent-solubilized (Supplementary Fig.3) and nanodisc-reconstituted (Fig.4) mutants at basic and acidic pH values. In nanodiscs, disruption of the charge-relay network promotes the inward-open conformation at both pH values regardless of which residue is mutated, as expected from a tightly coupled charge network (Fig.4 black and red curves). The addition of Hoechst 33342 to these mutants does not exclusively stabilize the outward-open state, unlike the “wild-type” protein where the charge network is intact (Fig.4 blue curves).

In contrast, the effects of the R72K and D128N mutations in detergent micelles are negligible at basic pH, and only appear at acidic pH (Supplementary Fig.3). The distinct effects in detergent micelles compared to nanodiscs may reflect a weaker coupling of this relay in the absence of lipids. These findings underscore the key role of this charge relay in the protonation-dependent conformational switch in LmrP and demonstrate that disruption of this network biases the energy landscape by changing the relative stability of the two conformations.

Lipid headgroups modulate the conformational equilibrium

Phosphatidylethanolamine (PE) has been reported to be required for the transport activity of LmrP [40]. We therefore investigated whether the presence of PE can account for the differences in the pH response between detergent and lipids. DEER distance measurements were performed in nanodiscs of defined composition, using synthetic lipids with different polar headgroups.

We first evaluated the potential effects of the fatty acid chain structure on the conformational equilibrium of LmrP by comparing distance distributions in lipids of either i) *E.coli* polar extract, ii) a mixture of 67% PE extracted from *E.coli* (variable fatty acid chains), 23% phosphatidylglycerol (PG) and 10 % cardiolipin (CL) or iii) a mixture of synthetic DOPE (67%) - DOPG (23%) - CL (10%). We observed that the structure and length of the fatty acid chain have only minor effects on the distance distributions of the extracellular and cytoplasmic reporters (Fig.5). Furthermore, the pH- and substrate-dependence of the distance distributions are similar in nanodiscs composed of these different lipid mixtures.

We then investigated whether the headgroup, specifically the protonation state of PE, is important in modulating LmrP conformational equilibrium. For this purpose, we reconstituted the extracellular and cytoplasmic distance reporters in nanodiscs containing PE with various degree of methylation of the headgroup amine, namely DOPE (no methylation), DOPE$(Me)_2$ (two methylations) and DOPC (fully methylated) while maintaining DOPG at 23%

and CL at 10%. Distance distributions obtained at pH5, pH6, pH7 and pH8 uncover a direct correlation between the degree of protonation of the ethanolamine headgroup and the population of the outward-open conformation (Supplementary Fig.4). To quantitatively assess this effect, we determined ΔG^0 of the transition between the inward- and outward-facing conformations as a function of pH in each lipid mixture, with the approximation that the transition from inward-open to outward-open conformation is two-state. The raw DEER data were fit using global analysis and the ratios of the populations of the two states were determined and used to calculate ΔG^0 (Fig.6).

The methylation of PE headgroup leads to stabilization of the outward-open conformation with the strongest effect observed for nanodiscs composed of DOPC-DOPG-CL (Fig.6 - orange bars). The stabilizing effect of the incremental methylation is enhanced at higher pH: at pH5, the outward-open conformation is not favored in any lipid compositions, while at pH8 it is favored in the DOPE$(Me)_2$-DOPG-CL and DOPC-DOPG-CL nanodiscs. At intermediates pHs, pH6 and pH7, the effects are distinct, suggesting that in this range of pH, the transporter is very sensitive to the presence/absence of protons on the polar headgroup.

Cardiolipin favors closing of the extracellular side

Considering the relative size of the nanodiscs and the transporter, the observed conformational regulation of LmrP by lipids is unlikely to be due to the bulk properties of the bilayer [41]. Rather we speculated that specific lipid-protein interactions are at play involving select lipids such as PE. One approach to test such interaction is the identification of endogenous lipid species with high affinity for the target protein. We therefore utilized ion mobility mass spectrometry (IM-MS) to analyze detergent-solubilized LmrP under increasing voltage which removes the detergent shell [42-45]. At 225 V of collisional activation, the protein is released from its detergent micelle, but still displays significant spectral heterogeneity (Fig.7 a). Although little free protein is detected, a distinct pattern is observed which shows peaks of regular spacing, suggesting the presence of relatively stable lipid-proteins adducts. By gradually increasing the collisional activation from 225 V up to 300 V, the heterogeneity of

the protein signal is decreased due to ejection of the bound lipids and singly charged species in the mass range around 1440 m/z stand out in the spectrum (Supplementary Fig 5). Comparing their masses to a lipid database allowed us to identify these species as a broad range of different CLs, establishing a strong interaction between LmrP and this class of lipids that withstands detergent solubilization and remains bound under the energetic conditions required for the MS analysis.

To elucidate whether the high affinity binding of CL to the protein is associated with a role in the conformational equilibrium, we performed distance measurements on a cytoplasmic and an extracellular distance reporters in a lipid mixture devoid of CL (i.e. DOPE-DOPG) at four different pH values, ranging from pH5 to pH8, as described in the previous section. Remarkably, we observed that the presence of CL affects the conformational equilibrium, but solely on the extracellular side (Fig.7 b). These findings indicate that the intracellular and extracellular sides of the transporter can rearrange independently, as previously shown [31], and that a specific lipid species—such as CL—might play a role in the decoupling of the conformational change between both sides.

Discussion

The main finding of this study is that lipid-protein interactions regulate the ion and substrate-dependent conformational dynamics of a secondary transporter. We show that the elements of alternating access are conserved in detergent micelles and lipid bilayers: the inward-facing and outward-facing conformations, as defined by patterns of distances between spin labels, are similar and the proton-dependent switch is maintained [31]. However, the presence of lipids shapes the energetics of alternating access by altering the relative stability of the two conformations. Whereas relatively acidic pH values were required to observe the distance peak(s) characteristic of the inward-open conformation in detergent micelles, the same peak(s) are present at neutral to basic pH in nanodiscs. Consequently, the apparent pK of the conformational transition is shifted towards neutral pH in lipid bilayers. As *L. lactis* typically thrives in pH range 6-7 [46,47], the lipid environment would enable the coexistence of the conformational intermediates at pH values closer to physiological pH. Conversely, the conformational transition would be very unlikely under physiological conditions if the pK is close to the acidic values observed in detergent.

Direct interactions between phospholipid headgroups and LmrP stabilize specific conformations. Our data unequivocally reveals a dependence of the equilibrium between inward-facing and outward-facing conformations on the headgroup of surrounding phospholipids. In particular, PE was shown to selectively stabilize the inward-facing conformation while CL promotes the uncoupled closing of the extracellular side. How might this change in relative stability of conformers be achieved?

Insight into the mechanism by which PE shifts the conformational equilibrium was obtained from the finding that the systematic substitution of the amine protons by methyl groups favors the outward-open conformation, indicating a direct coupling between the availability of protons on the headgroup and the shift in equilibrium. One interpretation of this result is that direct hydrogen bond(s) between the headgroup and the transporter plays a role in the conformational regulation. Such modulation of the conformational equilibrium through

direct hydrogen bonding with the phospholipids has been suggested for other membrane transport proteins such as the lactose permease LacY [48], the branched chain amino acid transport system from *S.cremoris* [49], the mechanosensitive channel MscL [50], and LmrP itself [40].

Despite its effect on the energetics of LmrP conformational equilibrium, no high affinity bound PE was identified by IM-MS. Unexpectedly, these measurements revealed the presence of several molecules of CL bound to LmrP, indicating a specific interaction. It is likely that the absence of bound PE may reflect its relatively small fraction in *L. Lactis* membranes [37,49]. Remarkably, binding of CL was correlated with a direct structural effect manifested by the closing of the extracellular side independent of an apparent movement on the intracellular side.

Extensive studies have explored the role of CL in the regulation of transporter function and pointed out its implication in the bioenergetics of the cell. CL displays increased affinity for all membrane proteins involved in ATP synthesis in the mitochondrion of eukaryotes and the plasma membrane of prokaryotes (reviewed in [51]). In addition, CL molecules are often observed in the crystal structures of mitochondrial membrane proteins [52-55] and have been suggested to take an active part in proton uptake [56,57]. Early studies assigned a pKa_2 of ~7 to one of the phosphate groups, a value that would allow CL to play a role as a versatile proton donor/acceptor and bind protons from the extracellular side [58,59]. Although the physiological roles of this unusual lipid continue to be elusive, the observation that high affinity interaction with CL is associated with closing of the extracellular side of LmrP is consistent with a proton donor role for this lipid, which would facilitate the protonation of acidic residues.

A conserved charge network control pH response and likely mediate interaction with lipids. Based on the structure of the multidrug transporter YajR (Fig.4 a), the interaction between the conserved Asp73 (Asp68 in LmrP) and the backbone of helix 11 appears to stabilize the outward-open conformation. This contention is supported by the changes

observed in the distances distributions upon D68 mutation (Fig.4 and Supplementary Fig.3), which consistently favors the inward-open conformation independent of the biochemical conditions (pH and/or lipids).

We speculate that the lipid-mediated shift in the equilibrium towards the inward-open state reflects an increase in the pK_a of D68 that is caused by a direct interaction between the phospholipid headgroup and the regulatory motif. This model is consonant with a number of evidence including the recent demonstration of conformational rearrangements of the ammonia transporter AmtB as a consequence of a direct interaction between a motif and PG bound with high-affinity [13]. Furthermore, a direct interaction through hydrogen bonding between PE headgroup and the aspartate 68 has already been suggested for the MFS symporter LacY based on computational studies in lipid bilayers composed of PE with various degree of methylation [60]. Functional studies carried out on LmrP D68C mutant reconstituted in proteoliposomes of various lipid compositions lead to a similar conclusion [40].

A balance between lipid-protein interactions and intra-protein interactions regulates the conformational equilibrium. The YajR structure shows that the key aspartate is positioned to participate in a charge relay with two conserved residues, arginine 77 and aspartate 126, in addition to its interaction with TM11 (Fig.4 a). We propose that the origin of the lipid-mediated stabilization of the inward-facing conformation of LmrP is a specific interaction between the aspartate 68, the charge relay and the headgroup that weakens the interaction with TM11. Our data indicate that the coupling between the residues of the charge relay motif is stronger in a lipid environment, supporting the hypothesis of an extended network involving a lipid headgroup. In contrast, detergent micelles would favor the interaction of D68 with TM11 at high pH thus explaining the lack of effects of R72K and D128N mutations on the conformational equilibrium at basic pH.

Concluding remarks. Our work provides a perspective on the role of lipids in the conformational dynamics of a membrane transporter, and thereby emphasizes that interactions with the membrane are a key determinant that has to be accounted for in the

elucidation of the mechanism(s) of transporters. The model that emerges from our data hypothesizes a direct interaction of lipid headgroups with charged residues to modulate the energetic of alternating access. Whether or not this mechanism can be extended to other transporters energized by a proton gradient remains to be investigated. We surmise that the strategy used here, where intramolecular distances are measured in detergent and in nanodiscs at various pH values, can be applied to a variety of such systems in order to test the role of lipid-protein interactions.

Methods

LmrP homology models. For each of the four structural templates (EmrD, PDB entry: 2GFP, LacY PDB: 2V8N, FucP PDB: 3O7Q and YajR PDB:3WDO), the sequence of LmrP was aligned using multiple alignments of LmrP and orthologs together with the sequences of the template and its orthologs. Initial alignments were generated using ClustalW [61], and then manually adjusted to i) prevent insertion and deletion in the TM helices and ii) avoid introduction of charged residues facing the lipid tails. Subsequent LmrP-template sequence alignments were then used to generate molecular models with Modeller [62]. Figures were prepared with Chimera [63].

Design and construction of the mutants. Cysteine-replacement residues were selected to be located at the extracellular or cytoplasmic end of a chosen TM region by using the homology models, while avoiding mutation of conserved residues. The mutations were introduced in C-terminally His-tagged LmrP in a derivative of the *E.coli* PCR®4 Blunt-TOPO® vector (Invitrogen) by site-directed mutagenesis using the QuikChange Lightning kit (Stratagene). The endogenous cysteine 270 was previously replaced by an alanine using the same method. After transformation, plasmid DNA was extracted and verified by sequencing. The *lmrp* gene fragment containing the desired mutation was then introduced into the pHLP5-3C vector, a derivative of the *L. lactis* expression vector pHLP5 containing C-terminally His-tagged LmrP [36]. After electroporation into NZ9000 *L. lactis* cells, the sequence was verified once again.

Bacterial strains, plasmids and growth conditions. The *L. lactis* NZ9000 was used as a host for pHLP5-3C based plasmid expression, as described previously [40,64,65]. Briefly, cells were grown at 30 °C in M17 medium supplemented with 0.5 % glucose and 5 mg.mL^{-1} chloramphenicol until the OD_{660} reached 0.8. Overexpression of LmrP mutants was then induced by addition of 1:1000 dilution of the supernatant of the nisin producing *L. lactis* strain NZ9700 [66]. After 2 hours of induction, cells were harvested by centrifugation at 5,000×*g*

LmrP mutants purification and labeling. Cells were washed in 50 mM HEPES, pH7 and resuspended (10 mL for each L of culture) in the same buffer containing 5 $mg.mL^{-1}$ of lysozyme, 10 $\mu g.mL^{-1}$ of DNAse I and 10 mM of $MgSO_4$. After 1-hour incubation at 30 °C, cells were broken by four passes at ~15,000 psi using a high pressure homogenizer. Cell debris and undisrupted cells were subsequently removed by three 15min centrifugations at 14,000×*g*. Inside-out membrane vesicles were then isolated by ultracentrifugation at 125,000×*g* for 2.5h at 4 °C and resuspended in 50 mM HEPES pH7, 150 mM NaCl and 10 % (v/v) glycerol (10 mL per L of cells). Inside-out membrane vesicles were solubilized with 1.2 % (w/v) β-dodecylmaltoside in the presence of 1 mM DTT for 1.5h at 4 °C on a rotating wheel. The insoluble fraction was then removed by ultracentrifugation at 125,000×*g* for 1h and the supernatant was batch-incubated for 2h with previously equilibrated Ni-NTA resin (25 μL resin per mL supernatant) in the presence of 10 mM imidazole. The slurry was then transferred to a column, the flow-through discarded, and the resin washed with 8 volumes of buffer A (50 mM HEPES pH7, 100 mM NaCl, 0.05 % (w/v) β-DDM and 20 mM imidazole), after which the protein was eluted by stepwise addition of buffer B (buffer A containing 250 mM imidazole). The concentration of the protein was determined by UV absorbance measurement at 280 nm. Spin-labeling was performed by adding a 30-fold molar excess of MTSSL (Enzo Life Sciences) from a 100 μM stock solution in DMF. The reaction was kept in the dark and at room temperature for 2h, and the process was repeated, followed by overnight incubation on ice. The protein was then run on a SDX-200 (GE Healthcare) size-exclusion chromatography column in HEPES buffer (50 mM HEPES pH8, 150 mM NaCl, 10 % (v/v) glycerol and 0.02 % (w/v) β-DDM).

MSP1E3D1 production and purification. Membrane scaffold protein (MSP1D1E3) was expressed and purified as described earlier [39,67] with the following modifications. Briefly, *E.coli* BL21 (DE3) cells containing the MSP1D1E3 gene in pET-28a(+) were plated on LB-agar plates supplemented with kanamycin (30 $\mu g.mL^{-1}$). A single colony was used to inoculate 30 mL of LB supplemented with 30 $\mu g.mL^{-1}$ of kanamycin. A dense overnight

culture of 30 mL was used to inoculate secondary culture of 1L Terrific broth supplemented with 30 μg.mL^{-1} of kanamycin. Cultures were grown at 37°C with shaking to an OD_{600} of ~2.2–2.5, then the expression of MSP1D1E3 was induced by addition of 1 mM IPTG (Inalco). Cultures were further grown for 4h at 37°C, and cells were harvested by centrifugation. Cell pellets were resuspended in 30 mL of lysis buffer (20 mM sodium phosphate, 1% Triton X-100, pH7.4), including 1/3 of a Complete EDTA-free protease inhibitor cocktail tablet (Roche), 10 μg.mL^{-1} of DNase I, and 10 mM of $MgSO_4$, and were lysed by 4 passes at 15000 psi in a high pressure homogenizer (Emulsiflex®). The lysate was centrifuged at 30,000×*g* for 30 min, and the supernatant was mixed with 3 mL of Ni-NTA resin equilibrated with lysis buffer. The slurry was transferred to a column and the flow-through discarded. The resin was washed with four bed volumes of buffer A (40 mM Tris/HCl, 0.3 M NaCl, pH8.0) containing 1% Triton X-100 , four bed volumes of buffer A containing 50 mM sodium cholate, four bed volumes of buffer A containing 20 mM imidazole, four bed volumes of buffer A containing 50 mM imidazole. The bound protein was eluted step-wise with buffer A containing 300 mM imidazole. The eluted MSP1D1E3 was passed over a desalting column into MSP buffer (50 mM Tris/HCl, 0.1M NaCl, 0.5 mM EDTA, pH7.5) and the concentration was determined by absorbance at 280 nm (extinction coefficient = 29,910 M^{-1} cm^{-1}). The protein was concentrated to ~15 mg.mL^{-1} on 10K MWCO concentrator (Amicon). The purity was assessed by SDS-PAGE and Coomassie staining.

Lipids preparation for nanodiscs. Lipids dissolved in chloroform (Avanti polar lipids) were combined to reach a final quantity of 100 mg, dried under nitrogen flow and then desiccated overnight under vacuum. The lipid films were hydrated with MSP buffer to reach a final concentration of 40 mg.mL^{-1}. β-DDM was added to the mixture to reach a final concentration of 7.5% (w/v). The lipids were further homogenized by low power sonication (160W) in Bioruptor ® for 5 min, with 30s ON - 30s OFF cycles, aliquoted and stored at -80 °C.

Reconstitution of LmrP in nanodiscs. For reconstitution into nanodiscs, spin-labeled LmrP mutants in β-DDM micelles were mixed with the appropriate lipid mixture, MSP1D1E3 and β-

DDM in the following molar ratios:lipid:MSP1D1E3, 60:1; MSP1D1E3:LmrP, 8:1; β - DDM:lipid, 3:1. Mixtures were rocked at room temperature for 30 min then incubated overnight at 4°C with rocking. In the morning, Biobeads SM-2 (700 $mg.mL^{-1}$) (Biorad) were added to the mixture, and incubated for 2h at 4°C then 1h at RT. The removal of the Biobeads was achieved by low speed centrifugation of the eppendorf containing the nanodisc assembly perforated with a needle to form a tiny hole. Nanodiscs were purified from undesirable species by size-exclusion chromatography on a superdex200 column (GE). Nanodiscs were concentrated using Amicon Ultra-50K centrifugal filter units at a speed not exceeding 1000*xg*. Nanodiscs containing the LmrP mutants were then characterized using SDS-PAGE to verify reconstitution and estimate reconstitution efficiency. As a complementary measurement, concentration of spin-labeled mutants in nanodiscs was determined as described previously [35] by comparing the intensity of the integrated CW-EPR spectrum to that of the same mutant in detergent micelles. The reconstitution efficiency was estimated to be 30%.

Preparation of the sample for DEER measurements. The protein in detergent micelles or reconstituted in nanodiscs was concentrated using a 50K MWCO concentrator to a spin label concentration of 100–150 μM (determined by the integration of the CW spectrum) after which glycerol was added to a final concentration of 23 % (v/v). For measurements performed at pHs other than pH8, two strategies were used. For the detergent-solubilized protein, an additional run on a desalting column was performed after size-exclusion chromatography and prior to concentration in order to exchange the buffer from HEPES pH8 to the appropriate buffer set at the right pH (MES-acetate 50 mM buffer for acidic pH values). Another strategy had to be used for the nanodiscs samples, as they tend to be unstable under acidic conditions and could not be concentrated as such. Consequently, an appropriate amount of acetic acid at 0.5M was added to the concentrated sample to lower its pH, which was checked with pH-paper. Where appropriate, Hoechst 33342 or Ethidium Bromide was added to a final concentration of 1 mM.

EPR measurements. DEER measurements were performed on a Bruker 580 pulsed ESR spectrometer operating at Q- band (33.4 GHz) using a standard four pulse protocol [68-70]. Data was collected with the samples at 83 K with 23 % (v/v) glycerol as cryoprotectant. Analysis of the DEER data to determine the distance distributions was carried in DeerAnalysis2011 or DeerAnalysis2013 [71]. The data was fit with Tikhonov regularization and L-curve determination of the optimal regularization parameter. Optimal background correction was established by statistical analysis of the fits. For a few samples, we observed evidence of partial protein aggregation [69]. This was manifested in the raw DEER decays by a deviation of the baseline from a stretched exponential and the lack of an oscillation in the echo decay even at longer collection times. Aggregation results in a component at the tail end of the distance distribution. The artifactual nature of these peaks (marked with an asterisk) could thus be demonstrated by varying the measured duration of the echo intensity oscillation. For the combined analysis of the DEER data a home-written software operating in the Matlab environment was used [38,39,72].The software assumes that the distance distribution consists of a sum of Gaussians and that the amplitudes of the components are allowed to vary across the physiological conditions, e.g. pH and lipid composition. For the ΔG^o calculation, the amplitudes of the fits that describe the outward facing or inward facing structures are obtained. The two amplitudes are then compared to obtain a K_{eq} for the two states for each pH and lipid condition. The K_{eq}'s are then used to obtain the ΔG^o. The error bars are obtained by propagating the fit errors for the individual amplitudes. The analysis of the raw DEER data is presented on Supplementary Fig.7.

MS measurements. Purified LmrP in detergent micelles was buffer exchanged into 100 mM ammonium acetate buffer pH6.8 supplemented with 0.02% n-dodecyl-β-D-maltoside using a G25 Sephadex column (GE lifesciences). Samples were introduced into the vacuum of the mass spectrometer using nano-electrospray ionization with in-house prepared gold-coated borosilicate glass capillaries using a spray voltage of +1.6 kV. Spectra were recorded on a quadrupole TOF instrument (Q-TOF2, Waters, Manchester, UK) modified for transmission of

native, high m/*z* protein assemblies, as described elsewhere [73]. Critical voltages and pressures throughout the instrument were 100 V and 225 V for the sampling cone and collision voltage respectively, with pressures of 15 and $2E^{-2}$ mbar for the source and collision cell. For the identification of the CL lipids a Synapt G2 (Waters, Manchester, UK) instrument was used due to the increased mass resolution at lower m/*z* values. Critical settings were sampling cone 200 V, 200 V trap collision energy, 10 V trap DC bias and 75 transfer collision energy. Pressures throughout the instrument were 6.5 and 2.6 E^{-2} mbar for the source and trap/transfer collision cells. All spectra were processed using Masslynx v4.1 (Waters).

Acknowledgments

We thank Drs Derek Claxton, Reza Dastvan and Daniel Hilger for critically reading the manuscript and Jean-Marie Ruysschaert for helpful discussions.

This work was supported by the Fonds de la Recherche Scientifique F.R.S.-F.N.R.S. (grant F.4523.12 - to C.G) and the NIH (grant R01GM077659 - to H.S.M)

C.M. is a Research Fellow of the F.R.I.A

C.G. is a Research Associate of the F.R.S.-F.N.R.S and a Welbio Investigator.

Author Contributions

C.M., H.M. and C.G.: experimental design. M.M, S.M. and C.M: mutagenesis, expression, activity, purification, reconstitution and labeling experiments. R.S: EPR measurements. R.S, C.M and H.M.: DEER data analysis. C.G. and C.M.: molecular modeling. A.K. and F.S.: MS measurements and data analysis. C.G. and H.M. oversaw all aspects of the experiments and manuscript preparation. All authors participated in interpreting the data and writing the paper.

Competing Financial Interests Statement

The authors declare no competing financial interests.

References

1. Singer, S.J. & Nicolson, G.L. The fluid mosaic model of the structure of cell membranes. *Science* **175**, 720-31 (1972).
2. Heijne, G. The distribution of positively charged residues in bacterial inner membrane proteins correlates with the trans-membrane topology. *EMBO J* **5**, 3021-7 (1986).
3. Cantor, R.S. The influence of membrane lateral pressures on simple geometric models of protein conformational equilibria. *Chem Phys Lipids* **101**, 45-56 (1999).
4. Powl, A.M., East, J.M. & Lee, A.G. Anionic phospholipids affect the rate and extent of flux through the mechanosensitive channel of large conductance MscL. *Biochemistry* **47**, 4317-28 (2008).
5. Phillips, R., Ursell, T., Wiggins, P. & Sens, P. Emerging roles for lipids in shaping membrane-protein function. *Nature* **459**, 379-85 (2009).
6. Dowhan, W. & Bogdanov, M. Lipid-protein interactions as determinants of membrane protein structure and function. *Biochem Soc Trans* **39**, 767-74 (2011).
7. Hanson, M.A. et al. A specific cholesterol binding site is established by the 2.8 A structure of the human beta2-adrenergic receptor. *Structure* **16**, 897-905 (2008).
8. Hunte, C. & Richers, S. Lipids and membrane protein structures. *Curr Opin Struct Biol* **18**, 406-11 (2008).
9. Lee, A.G. Lipid-protein interactions in biological membranes: a structural perspective. *Biochim Biophys Acta* **1612**, 1-40 (2003).
10. Contreras, F.X. et al. Molecular recognition of a single sphingolipid species by a protein's transmembrane domain. *Nature* **481**, 525-529 (2012).
11. Lee, A.G. Lipid-protein interactions. *Biochem Soc Trans* **39**, 761-6 (2011).
12. Vitrac, H., Bogdanov, M. & Dowhan, W. Proper fatty acid composition rather than an ionizable lipid amine is required for full transport function of lactose permease from Escherichia coli. *J Biol Chem* **288**, 5873-85 (2013).
13. Laganowsky, A. et al. Membrane proteins bind lipids selectively to modulate their structure and function. *Nature* **510**, 172-5 (2014).
14. Pliotas, C. et al. The role of lipids in mechanosensation. *Nat Struct Mol Biol* **22**, 991-8 (2015).
15. Koshy, C. et al. Structural evidence for functional lipid interactions in the betaine transporter BetP. *EMBO J* **32**, 3096-105 (2013).
16. Dawaliby, R. et al. Allosteric regulation of G protein-coupled receptor activity by phospholipids. *Nat Chem Biol* (2015).
17. Hamilton, P.J. et al. PIP2 regulates psychostimulant behaviors through its interaction with a membrane protein. *Nature Chemical Biology* **10**, 582-589 (2014).
18. Khelashvili, G. & Weinstein, H. Functional mechanisms of neurotransmitter transporters regulated by lipid-protein interactions of their terminal loops. *Biochimica Et Biophysica Acta-Biomembranes* **1848**, 1765-1774 (2015).
19. Khelashvili, G., Galli, A. & Weinstein, H. Phosphatidylinositol 4,5-Biphosphate (PIP2) Lipids Regulate the Phosphorylation of Syntaxin N-Terminus by Modulating Both Its Position and Local Structure. *Biochemistry* **51**, 7685-7698 (2012).
20. Sachs, J.N. & Engelman, D.M. Introduction to the membrane protein reviews: the interplay of structure, dynamics, and environment in membrane protein function. *Annu Rev Biochem* **75**, 707-12 (2006).
21. Bolhuis, H. et al. Energetics and mechanism of drug transport mediated by the lactococcal multidrug transporter LmrP. *J Biol Chem* **271**, 24123-8 (1996).
22. Bolhuis, H. et al. The Lactococcal lmrP gene encodes a proton motive force-dependent drug transporter. *J Biol Chem* **270**, 26092-8 (1995).

23. Putman, M., van Veen, H.W., Degener, J.E. & Konings, W.N. The lactococcal secondary multidrug transporter LmrP confers resistance to lincosamides, macrolides, streptogramins and tetracyclines. *Microbiology* **147**, 2873-80 (2001).
24. Gottesman, M.M. & Pastan, I. Biochemistry of multidrug resistance mediated by the multidrug transporter. *Annu Rev Biochem* **62**, 385-427 (1993).
25. Putman, M., van Veen, H.W. & Konings, W.N. Molecular properties of bacterial multidrug transporters. *Microbiol Mol Biol Rev* **64**, 672-93 (2000).
26. Fluman, N., Ryan, C.M., Whitelegge, J.P. & Bibi, E. Dissection of mechanistic principles of a secondary multidrug efflux protein. *Mol Cell* **47**, 777-87 (2012).
27. Schaedler, T.A. & van Veen, H.W. A flexible cation binding site in the multidrug major facilitator superfamily transporter LmrP is associated with variable proton coupling. *FASEB J* **24**, 3653-61 (2010).
28. Schuldiner, S. EmrE, a model for studying evolution and mechanism of ion-coupled transporters. *Biochim Biophys Acta* **1794**, 748-62 (2009).
29. Paulsen, I.T., Brown, M.H., Littlejohn, T.G., Mitchell, B.A. & Skurray, R.A. Multidrug resistance proteins QacA and QacB from Staphylococcus aureus: membrane topology and identification of residues involved in substrate specificity. *Proc Natl Acad Sci U S A* **93**, 3630-5 (1996).
30. Kaatz, G.W. & Seo, S.M. Inducible NorA-mediated multidrug resistance in Staphylococcus aureus. *Antimicrob Agents Chemother* **39**, 2650-5 (1995).
31. Masureel, M. et al. Protonation drives the conformational switch in the multidrug transporter LmrP. *Nat Chem Biol* **10**, 149-55 (2014).
32. Claxton, D.P., Kazmier, K., Mishra, S. & McHaourab, H.S. Navigating Membrane Protein Structure, Dynamics, and Energy Landscapes Using Spin Labeling and EPR Spectroscopy. *Methods Enzymol* **564**, 349-87 (2015).
33. Pao, S.S., Paulsen, I.T. & Saier, M.H., Jr. Major facilitator superfamily. *Microbiol Mol Biol Rev* **62**, 1-34 (1998).
34. Jiang, D. et al. Structure of the YajR transporter suggests a transport mechanism based on the conserved motif A. *Proc Natl Acad Sci U S A* **110**, 14664-9 (2013).
35. Zou, P. & McHaourab, H.S. Increased sensitivity and extended range of distance measurements in spin-labeled membrane proteins: Q-band double electron-electron resonance and nanoscale bilayers. *Biophys J* **98**, L18-20 (2010).
36. Putman, M., van Veen, H.W., Poolman, B. & Konings, W.N. Restrictive use of detergents in the functional reconstitution of the secondary multidrug transporter LmrP. *Biochemistry* **38**, 1002-8 (1999).
37. Gbaguidi, B. et al. Proton motive force mediates a reorientation of the cytosolic domains of the multidrug transporter LmrP. *Cell Mol Life Sci* **61**, 2646-57 (2004).
38. Stein, R.A., Beth, A.H. & Hustedt, E.J. A Straightforward Approach to the Analysis of Double Electron-Electron Resonance Data. *Methods Enzymol* **563**, 531-67 (2015).
39. Mishra, S. et al. Conformational dynamics of the nucleotide binding domains and the power stroke of a heterodimeric ABC transporter. *Elife* **3**, e02740 (2014).
40. Hakizimana, P., Masureel, M., Gbaguidi, B., Ruysschaert, J.M. & Govaerts, C. Interactions between phosphatidylethanolamine headgroup and LmrP, a multidrug transporter: a conserved mechanism for proton gradient sensing? *J Biol Chem* **283**, 9369-76 (2008).
41. Denisov, I.G., McLean, M.A., Shaw, A.W., Grinkova, Y.V. & Sligar, S.G. Thermotropic phase transition in soluble nanoscale lipid bilayers. *J Phys Chem B* **109**, 15580-8 (2005).
42. Lanucara, F., Holman, S.W., Gray, C.J. & Eyers, C.E. The power of ion mobility-mass spectrometry for structural characterization and the study of conformational dynamics. *Nat Chem* **6**, 281-94 (2014).
43. Barrera, N.P., Zhou, M. & Robinson, C.V. The role of lipids in defining membrane protein interactions: insights from mass spectrometry. *Trends Cell Biol* **23**, 1-8 (2013).
44. Zhou, M. et al. Mass spectrometry of intact V-type ATPases reveals bound lipids and the effects of nucleotide binding. *Science* **334**, 380-5 (2011).

45. Bechara, C. et al. A subset of annular lipids is linked to the flippase activity of an ABC transporter. *Nat Chem* **7**, 255-62 (2015).
46. Adamberg, K., Kask, S., Laht, T.M. & Paalme, T. The effect of temperature and pH on the growth of lactic acid bacteria: a pH-auxostat study. *Int J Food Microbiol* **85**, 171-83 (2003).
47. Bibal, B., Goma, G., Vayssier, Y. & Pareilleux, A. Influence of Ph, Lactose and Lactic-Acid on the Growth of Streptococcus-Cremoris - a Kinetic-Study. *Applied Microbiology and Biotechnology* **28**, 340-344 (1988).
48. Chen, C.C. & Wilson, T.H. The phospholipid requirement for activity of the lactose carrier of Escherichia coli. *J Biol Chem* **259**, 10150-8 (1984).
49. Driessen, A.J., Zheng, T., In't Veld, G., Op den Kamp, J.A. & Konings, W.N. Lipid requirement of the branched-chain amino acid transport system of Streptococcus cremoris. *Biochemistry* **27**, 865-72 (1988).
50. Powl, A.M., East, J.M. & Lee, A.G. Importance of direct interactions with lipids for the function of the mechanosensitive channel MscL. *Biochemistry* **47**, 12175-84 (2008).
51. Haines, T.H. A new look at Cardiolipin. *Biochim Biophys Acta* **1788**, 1997-2002 (2009).
52. Shintre, C.A. et al. Structures of ABCB10, a human ATP-binding cassette transporter in apo- and nucleotide-bound states. *Proc Natl Acad Sci U S A* **110**, 9710-5 (2013).
53. Pebay-Peyroula, E. et al. Structure of mitochondrial ADP/ATP carrier in complex with carboxyatractyloside. *Nature* **426**, 39-44 (2003).
54. Nury, H. et al. Structural basis for lipid-mediated interactions between mitochondrial ADP/ATP carrier monomers. *FEBS Lett* **579**, 6031-6 (2005).
55. Ruprecht, J.J. et al. Structures of yeast mitochondrial ADP/ATP carriers support a domain-based alternating-access transport mechanism. *Proc Natl Acad Sci U S A* **111**, E426-34 (2014).
56. Lange, C., Nett, J.H., Trumpower, B.L. & Hunte, C. Specific roles of protein-phospholipid interactions in the yeast cytochrome bc1 complex structure. *EMBO J* **20**, 6591-600 (2001).
57. Poyry, S. et al. Atomistic simulations indicate cardiolipin to have an integral role in the structure of the cytochrome bc(1) complex. *Biochimica Et Biophysica Acta-Bioenergetics* **1827**, 769-778 (2013).
58. Kates, M., Syz, J.Y., Gosser, D. & Haines, T.H. pH-dissociation characteristics of cardiolipin and its 2'-deoxy analogue. *Lipids* **28**, 877-82 (1993).
59. Haines, T.H. & Dencher, N.A. Cardiolipin: a proton trap for oxidative phosphorylation. *FEBS Lett* **528**, 35-9 (2002).
60. Lensink, M.F., Govaerts, C. & Ruysschaert, J.M. Identification of specific lipid-binding sites in integral membrane proteins. *J Biol Chem* **285**, 10519-26 (2010).

Methods References

61. Thompson, J.D., Higgins, D.G. & Gibson, T.J. CLUSTAL W: improving the sensitivity of progressive multiple sequence alignment through sequence weighting, position-specific gap penalties and weight matrix choice. *Nucleic Acids Res* **22**, 4673-80 (1994).
62. Webb, B. & Sali, A. Comparative Protein Structure Modeling Using MODELLER. *Curr Protoc Bioinformatics* **47**, 5 6 1-5 6 32 (2014).
63. Pettersen, E.F. et al. UCSF Chimera--a visualization system for exploratory research and analysis. *J Comput Chem* **25**, 1605-12 (2004).
64. Mazurkiewicz, P., Driessen, A.J. & Konings, W.N. Energetics of wild-type and mutant multidrug resistance secondary transporter LmrP of Lactococcus lactis. *Biochim Biophys Acta* **1658**, 252-61 (2004).
65. Putman, M., Koole, L.A., van Veen, H.W. & Konings, W.N. The secondary multidrug transporter LmrP contains multiple drug interaction sites. *Biochemistry* **38**, 13900-5 (1999).
66. Mierau, I. & Kleerebezem, M. 10 years of the nisin-controlled gene expression system (NICE) in Lactococcus lactis. *Appl Microbiol Biotechnol* **68**, 705-17 (2005).

67. Boldog, T., Li, M. & Hazelbauer, G.L. Using Nanodiscs to create water-soluble transmembrane chemoreceptors inserted in lipid bilayers. *Methods Enzymol* **423**, 317-35 (2007).
68. Jeschke, G. & Polyhach, Y. Distance measurements on spin-labelled biomacromolecules by pulsed electron paramagnetic resonance. *Phys Chem Chem Phys* **9**, 1895-910 (2007).
69. Jeschke, G. DEER distance measurements on proteins. *Annu Rev Phys Chem* **63**, 419-46 (2012).
70. Pannier, M., Veit, S., Godt, A., Jeschke, G. & Spiess, H.W. Dead-time free measurement of dipole-dipole interactions between electron spins. *J Magn Reson* **142**, 331-40 (2000).
71. Jeschke, G. et al. DeerAnalysis2006—a comprehensive software package for analyzing pulsed ELDOR data. *Applied Magnetic Resonance* **30**, 473-498 (2006).
72. Brandon, S., Beth, A.H. & Hustedt, E.J. The global analysis of DEER data. *J Magn Reson* **218**, 93-104 (2012).
73. Sobott, F., Hernandez, H., McCammon, M.G., Tito, M.A. & Robinson, C.V. A tandem mass spectrometer for improved transmission and analysis of large macromolecular assemblies. *Anal Chem* **74**, 1402-7 (2002).

FIGURE LEGENDS

Figure 1 | Ligand-dependent conformational changes of LmrP in lipid bilayers. DEER distance distributions for spin labeled cysteine pairs between the N- and C-lobes located on the extracellular (a) and cytoplasmic (b) ends of TM helices, obtained at pH8 (black), pH6 (red) and pH8 + 1mM Hoechst 33342 (blue). Distributions were normalized: r indicates interspin distance; *P(r)* indicates the distance probability, asterisks denote peaks resulting from partial aggregation observed in some samples upon concentration (see Methods). The closing or opening upon ligand binding is indicated by colored arrows (red: proton binding, blue: Hoechst 33342 binding) with targeted helices in orange. Left: LmrP homology model with cysteine pairs highlighted in red, connected by a line, with TM numbers indicated on top - view from the extracellular (a) or cytoplasmic (b) side. The N-lobe is colored blue and the C-lobe is colored grey.

Figure 2 | The lipid environment favors the inward-open conformation. DEER distance distributions of the $160R_1$-$310R_1$ and the $137R_1$-$349R_1$ pairs, used as extracellular (left) and cytoplasmic (right) reporters, respectively. Top: mutants reconstituted in *E.coli* polar lipids nanodiscs, at pH values ranging from pH5 to pH8.5 in 0.5 unit increments. Bottom: mutants in detergent micelles, at pH values ranging from pH4.5 to pH8 in 0.5 unit increments.

Figure 3 | The lipid environment increases the pK of LmrP conformational transition. The fraction of the inward-open component(s) of the distance distributions for the extracellular reporter ($160R_1$-$310R_1$, left) and cytoplasmic reporter ($137R_1$-$349R_1$, right), as determined by global analysis of the raw data, is plotted as a function of pH and fitted with a sigmoidal dose-response curve. The top and bottom panels represent the pH-dependence of the distance distribution in nanodiscs and detergent micelles, respectively.

Figure 4 | Disruption of the charge-relay network favors the inward-open conformation in nanodiscs. (a) a charge-relay network of conserved residues stabilizes the outward-open conformation of the LmrP homolog YajR. TM2 and TM11 are highlighted in orange. The

cytoplasmic domain of YajR was removed for clarity. (b) single mutations D68N, R72K and D128N were combined with extracellular ($160R_1$-$310R_1$) and (c) cytoplasmic ($137R_1$-$349R_1$) reporters. DEER measurements carried out at pH6 (red), pH8 (black), and pH8 + Hoechst 33342 (blue) in the absence (dashed line) and presence (solid line) of each mutation.

Figure 5 | Differences in the fatty acid chain length and structure cause minor changes of the conformational equilibrium. DEER distance distributions of the $160R_1$-$310R_1$ and the $137R_1$-$349R_1$ pairs, used as extracellular (left) and cytoplasmic (right) distance reporters, respectively. The distance distributions at pH8 (black), pH6 (red), pH8 + Hoechst 33342 (blue) are comparatively similar in (a) the *E.coli* polar lipid extract, (b) the combination of PE, PG and CL extracts of *E.coli*, and (c) the combination of synthetic DOPE, DOPG and CL.

Figure 6 | Incremental methylation of phosphatidylethanolamine headgroup stabilizes the outward-open conformation. ΔG^o of the transition were calculated and plotted as a function of the pH and the lipid composition. (a) extracellular distance reporter $160R_1$-$310R_1$. (b) cytoplasmic distance reporter $137R_1$-$349R_1$. In order of decreasing ΔG^o values: DOPE-DOPG-CL (grey)> DOPE$(Me)_2$-DOPG-CL (blue) > DOPC-DOPG-CL (orange). See methods for calculation of ΔG^o and associated errors.

Figure 7 | Cardiolipin binds to LmrP with high-affinity and highlights conformational decoupling between the two sides of the transporter. (a) Positive mode nano-ESI MS. Although a charge state distribution from 11^+ to 17^+ is observed, only the 13^+ and 15^+ peaks are indicated for clarity by dotted lines representing the theoretical m/z values, with red numbers corresponding to the number of CL molecules bound. The inset shows the deconvoluted mass spectrum revealing up to eight CL bound. The red dotted line indicates the mass of free LmrP. (b) distance distributions of the extracellular $160R_1$-$310R_1$ (top panels) and cytoplasmic $137R_1$-$349R_1$ (bottom panels) reporters reconstituted in nanodisc with (grey) and without (pink) 10% CL.

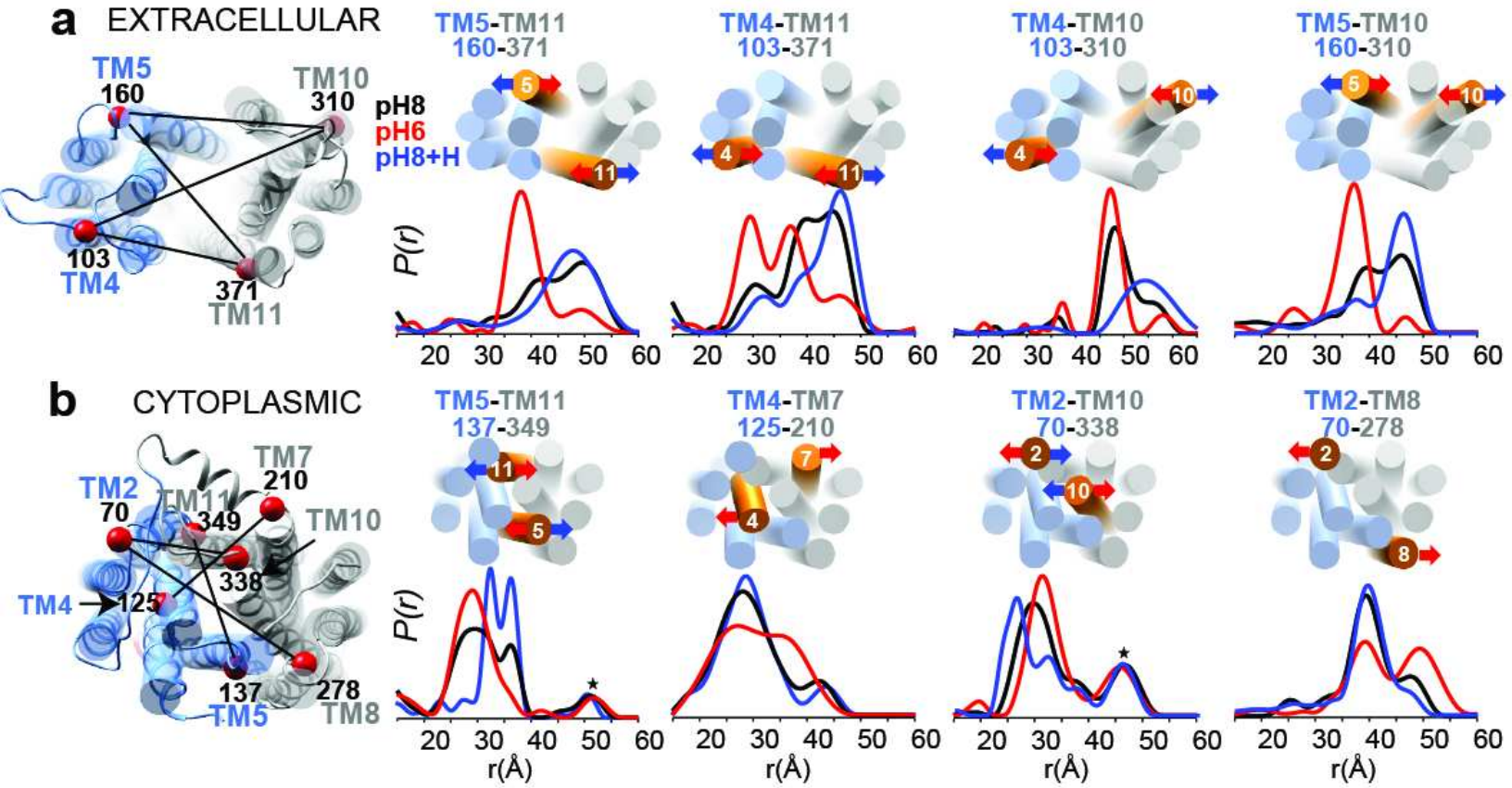
a
EXTRACELLULAR
TM5
160
TM10
310
103
TM4
371
TM11
pH8
pH6
pH8+H
TM5-TM11
160-371
TM4-TM11
103-371
TM4-TM10
103-310
TM5-TM10
160-310
P(r)
20 30 40 50 60
b
CYTOPLASMIC
TM7
210
TM2
70
TM11
349
TM10
338
TM4
125
137
278
TM5
TM8
TM5-TM11
137-349
TM4-TM7
125-210
TM2-TM10
70-338
TM2-TM8
70-278
r(Å)

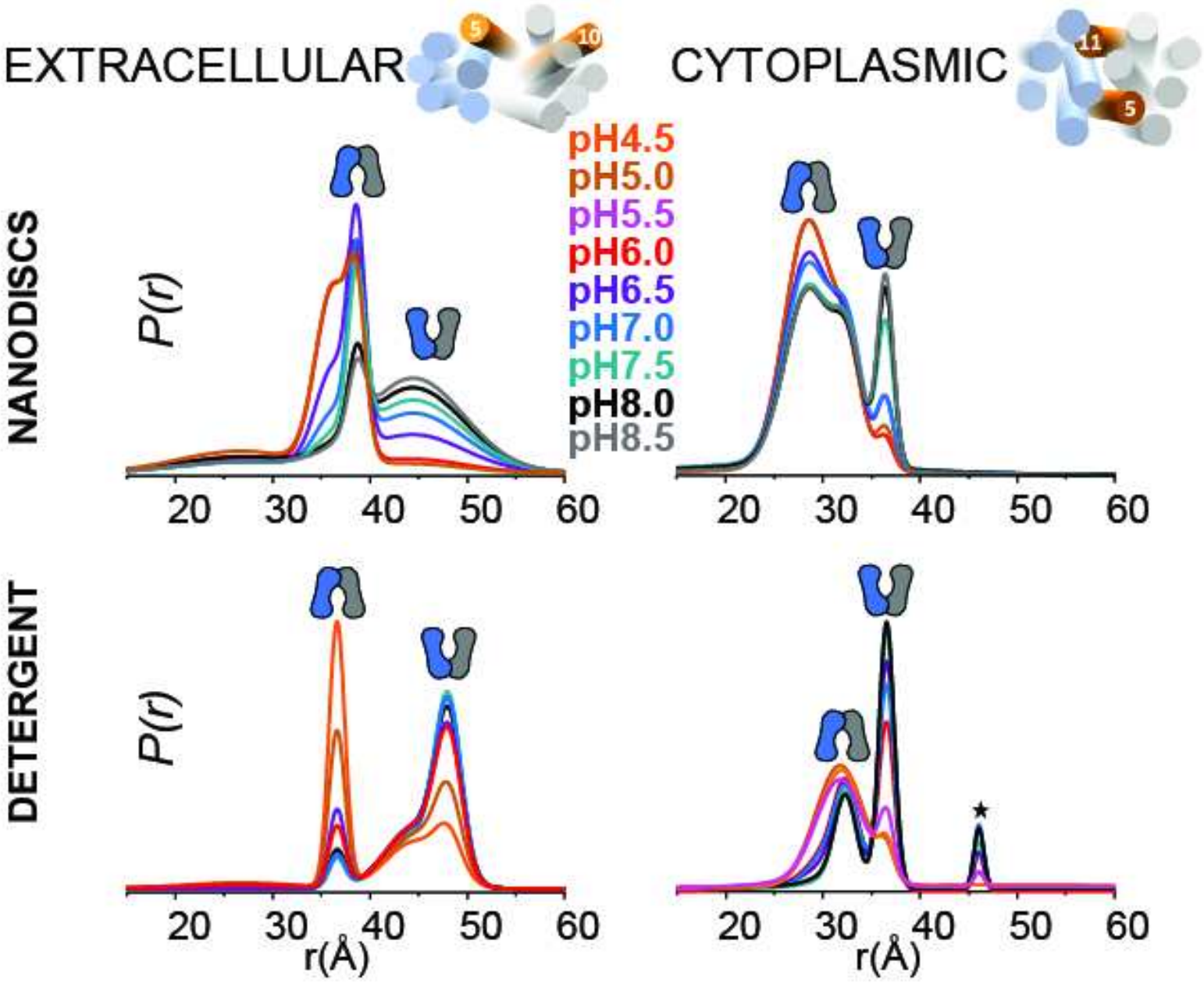
EXTRACELLULAR
5
10
CYTOPLASMIC
11
5
NANODISCS
DETERGENT
P(r)
pH4.5
pH5.0
pH5.5
pH6.0
pH6.5
pH7.0
pH7.5
pH8.0
pH8.5
20
30
40
50
60
r(Å)

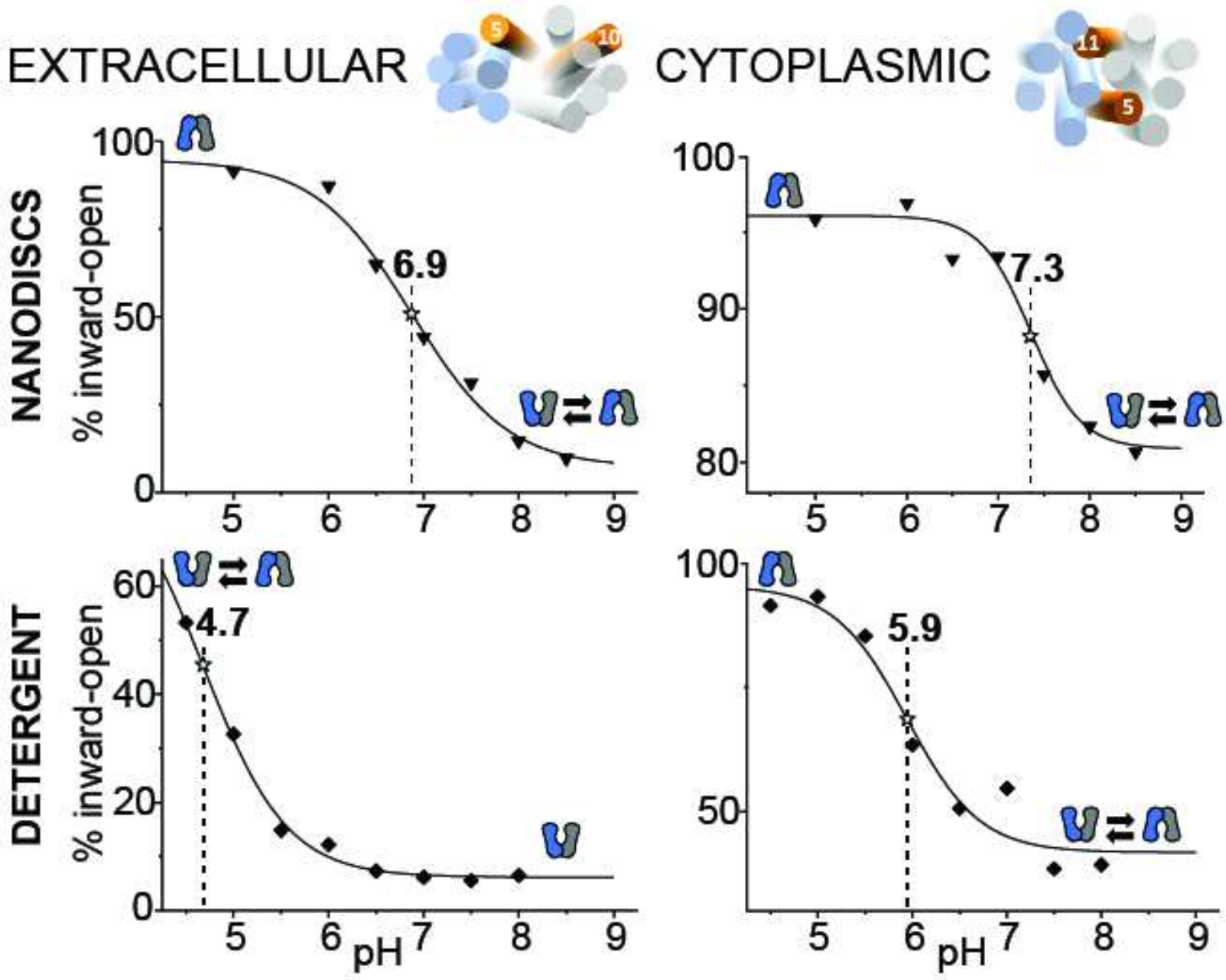
EXTRACELLULAR
CYTOPLASMIC
NANODISCS
DETERGENT
% inward-open
pH
6.9
7.3
4.7
5.9
100
50
0
90
80
60
40
20
5
6
7
8
9

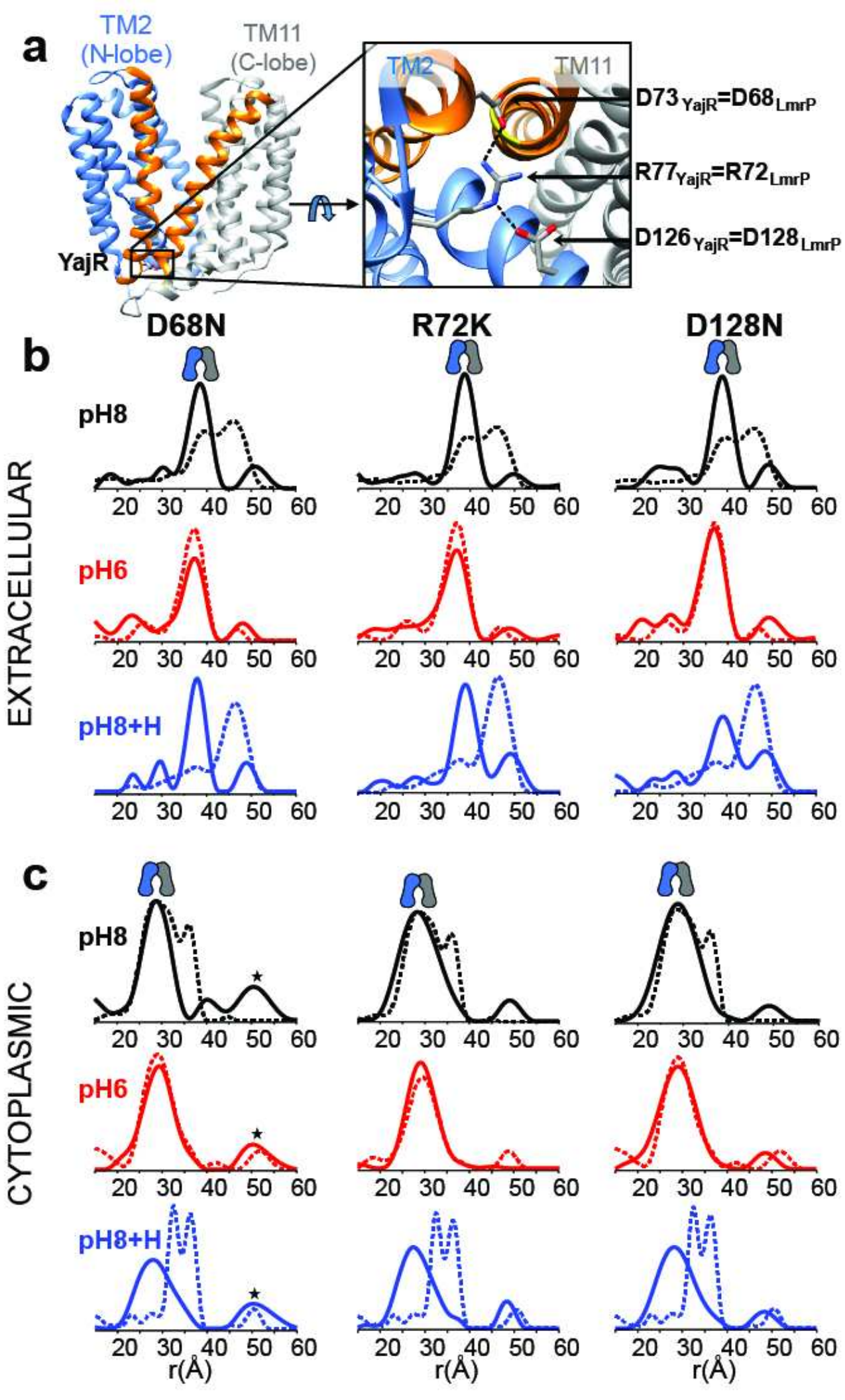
a
TM2
(N-lobe)
TM11
(C-lobe)
YajR
TM2
TM11
D73 YajR=D68 LmrP
R77 YajR=R72 LmrP
D126 YajR=D128 LmrP
D68N
R72K
D128N
b
EXTRACELLULAR
pH8
pH6
pH8+H
20 30 40 50 60
c
CYTOPLASMIC
pH8
pH6
pH8+H
20 30 40 50 60
r(Å)

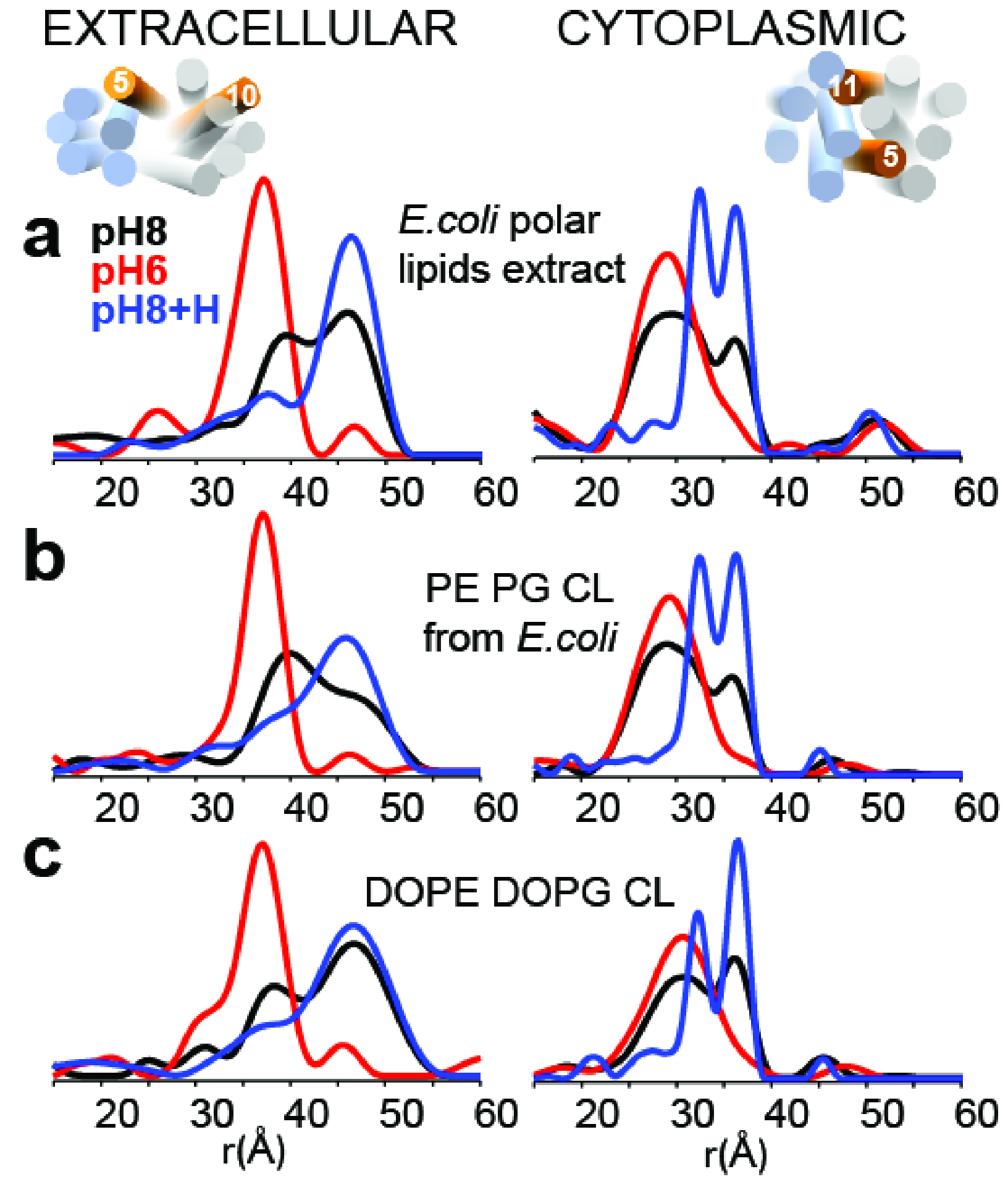
EXTRACELLULAR
CYTOPLASMIC
5
10
11
5
a
pH8
pH6
pH8+H
E.coli polar
lipids extract
20
30
40
50
60
b
PE PG CL
from E.coli
c
DOPE DOPG CL
r(Å)
r(Å)

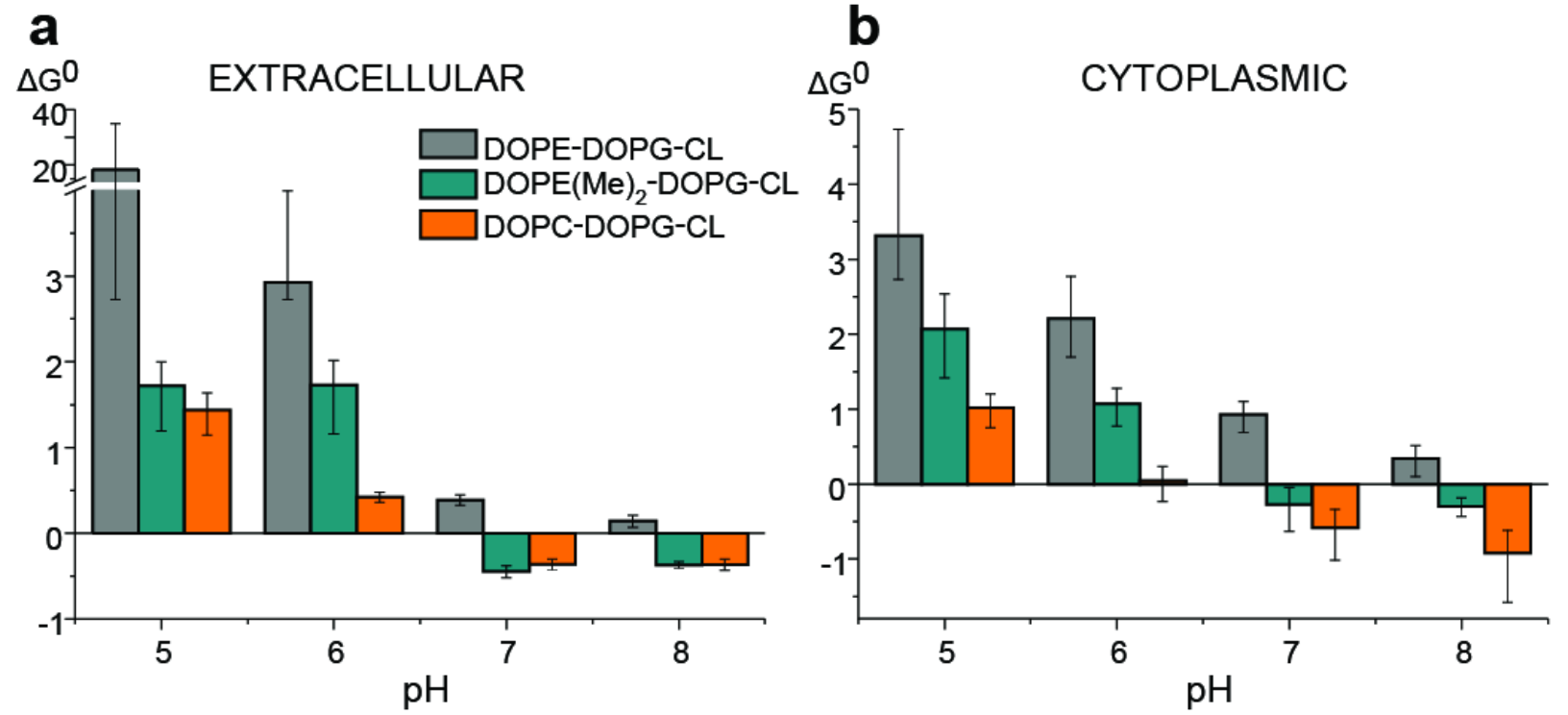
a
ΔG0
EXTRACELLULAR
40
20
3
2
1
0
-1
DOPE-DOPG-CL
DOPE(Me)2-DOPG-CL
DOPC-DOPG-CL
5
6
7
8
pH
b
ΔG0
CYTOPLASMIC
5
4
3
2
1
0
-1
5
6
7
8
pH

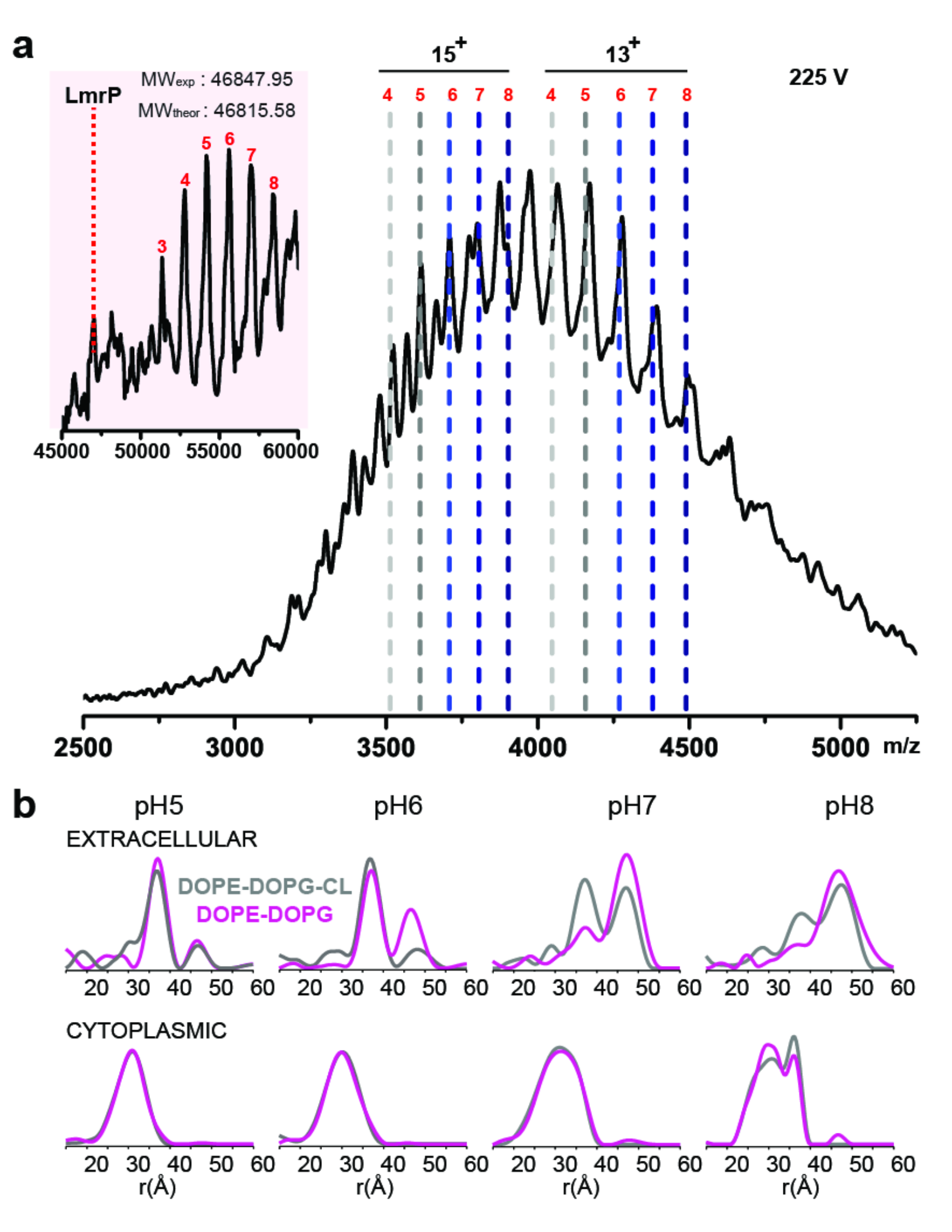
a
LmrP
MWexp : 46847.95
MWtheor : 46815.58
3
4
5
6
7
8
45000
50000
55000
60000
15+
13+
4
5
6
7
8
4
5
6
7
8
225 V
2500
3000
3500
4000
4500
5000
m/z
b
pH5
pH6
pH7
pH8
EXTRACELLULAR
DOPE-DOPG-CL
DOPE-DOPG
CYTOPLASMIC
20
30
40
50
60
r(Å)